Atmospheric
Chemistry
and Physics
Discussions

Open Access

Explaining variance in black carbon's aging timescale

L. Fierce[1], N. Riemer[2], and T. Bond[1]

[1]Department of Civil and Environmental Engineering, University of Illinois at Urbana-Champaign, Urbana, Illinois, USA
[2]Department of Atmospheric Sciences, University of Illinois at Urbana-Champaign, Urbana, Illinois, USA

Correspondence to: N. Riemer (nriemer@illinois.edu)

Discussion Paper | Discussion Paper | Discussion Paper | Discussion Paper |

ACPD

14, 18703–18737, 2014

Explaining variance in BC aging timescales

L. Fierce et al.

Title Page

Abstract	Introduction
Conclusions	References
Tables	Figures

|◄ | ►|

◄ | ►

Back | Close

Full Screen / Esc

Printer-friendly Version

Interactive Discussion

Abstract

The size and composition of particles containing black carbon (BC) are modified soon after emission by condensation of semi-volatile substances and coagulation with other particles, known collectively as "aging" processes. Although this change in particle properties is widely recognized, the timescale for transformation is not well constrained. In this work, we simulated aerosol aging with the particle-resolved model PartMC-MOSAIC and extracted aging timescales based on changes in particle cloud condensation nuclei (CCN). We simulated nearly 300 scenarios and, through a regression analysis, identified the key parameters driving the value of the aging timescale. We show that BC's aging timescale spans from hours to weeks, depending on the local environmental conditions and the characteristics of the fresh BC-containing particles. Although the simulations presented in this study included many processes and particle interactions, we show that 80 % of the variance in the aging timescale is explained by only a few key parameters. The condensation aging timescale decreased with the flux of condensing aerosol and was shortest for the largest fresh particles, while the coagulation aging timescale decreased with the total number concentration of large ($D > 100$ nm), CCN-active particles and was shortest for the smallest fresh particles. Therefore, both condensation and coagulation play important roles in aging, and their relative impact depends on the particle size range.

1   Introduction

Particles containing black carbon (BC) alter the Earth's energy balance by scattering and absorbing solar radiation (McCormick and Ludwig, 1967; Rosen et al., 1978; Schulz et al., 2006), by interacting with clouds (Twomey, 1977; Twomey et al., 1984; Lohmann et al., 2005; Albrecht, 1989; Ackerman et al., 2000), and by decreasing the albedo of ice and snow (Hansen and Nazarenko, 2004; Jacobson, 2004). Each of these climate effects depends on the properties of individual BC-containing particles and their

atmospheric residence time. The dominant removal mechanism of BC mass from the atmosphere is wet deposition (Cozic et al., 2007), with one important pathway being the activation of BC-containing particles into cloud condensation nuclei (CCN) and their subsequent removal if the cloud precipitates. Although freshly emitted BC-containing particles are too small and hydrophobic to activate (Maricq, 2007; Weingartner et al., 1997), their morphology and chemical composition are altered soon after emission by condensation of semi-volatile gases and coagulation with pre-existing particles (Johnson et al., 2005).

These changes in particle characteristics, termed "aging", often increase the particles' susceptibility to cloud droplet nucleation and wet removal (Furutani et al., 2008; Cantrell et al., 2001; Zuberi et al., 2005), so these processes must be included in global models. However, a complex aerosol population that evolves with time is not easily simulated in climate models, so even sophisticated aerosol schemes do not fully resolve particle properties (Jacobson, 1997; Wexler et al., 1994; Bauer et al., 2008; Binkowski and Roselle, 2003; McGraw, 1997). The simplest representation of aging classifies BC mass as either hydrophobic or hydrophilic, such that hydrophilic BC is susceptible to removal by wet deposition and hydrophobic BC is not. In this framework, BC is transferred from the hydrophobic (fresh) category to the hydrophilic (aged) category according to a first-order aging timescale (Cooke and Wilson, 1996; Croft et al., 2005; Koch, 2001). Global models apply a fixed aging timescale of 1–3 days. Global modeling studies have shown that estimates of BC's climate forcing are sensitive to the assumed aging timescale (Koch et al., 2009), but its value is not well constrained.

Other studies have developed parameterizations of BC's aging timescale that vary with environmental conditions. Liu et al. (2011) developed a parameterization of black carbon aging by condensation that depends on the condensation rate of sulfuric acid and overall BC surface area. They showed that, by allowing for slower aging in the winter, their parameterization was better able to represent seasonal variability in black carbon transport to the Arctic. Oshima and Koike (2013) extended this approach and developed a parameterization of aging timescales based on simulations with a box

model. Their parameterization predicted the rate for BC to transition from a hydrophobic class to a hydrophilic class, expressed as a function of the mass-normalized coating rate and on parameters of the fresh BC size distribution. Riemer et al. (2004) showed that timescales for aging by coagulation decrease with the overall aerosol number concentration, which they parameterized using a simple power law, and this parameterization was applied by Croft et al. (2005). Pierce et al. (2009) parameterized size-resolved coagulation rates as a first-order loss process that depends on the overall size distribution. In a detailed analysis of aging timescales in a specific urban environment, Riemer et al. (2010) showed that timescales for particles to transition from CCN-inactive to CCN-active varied diurnally due to variations in condensation aging rates. Because the timescale from Riemer et al. (2010) is based on changes in particle CCN activity, it quantifies changes in particle characteristics that these first-order aging models are meant to represent.

This study builds on the work of Riemer et al. (2010) to quantify how the CCN-based aging timescale varies with environmental conditions. In many climate models the aerosol microphysical schemes explicitly represent the evolution of aerosol size and composition. However, the practice of using a fixed aging time-scale is still widespread (Jo et al., 2013; Chin et al., 2014; Schmidt et al., 2014). Further, in addition to their application in climate models, parameterizations of aging timescales can be used as a diagnostic tool for analysis of aging processes.

We simulated aerosol dynamics for nearly 300 plume scenarios with a particle-resolved aerosol model and extracted aging timescales from the model results. Unlike other aerosol schemes, which simplify the representation of particle composition, the particle-resolved model tracks the composition of each simulated particle, so it is uniquely suited to study the impact of aging on per-particle CCN activity. The aging timescale varied by orders of magnitude, resulting from differences in emissions and environmental conditions between the scenarios. In this study, we apply a regression analysis to identify the set of independent variables that best explain this variance in BC's aging timescale.

2   Extracting aging timescales from particle-resolved model output

In a first-order model of aging, particles transition from fresh to aged according to an aging timescale, τ_{aging}. In this framework, some criterion must be applied to distinguish fresh and aged particles. Particle CCN activity at a specified environmental supersaturation is the aging criterion applied in this work, so the aging timescale indicates changes in particles' susceptibility to removal by wet deposition. We define aged particles as those that are activated at a specified environmental supersaturation, and fresh particles are CCN-inactive at that supersaturation threshold. The first-order aging model is given by:

$$\left[\frac{\mathrm{d}N_{\text{fresh}}}{\mathrm{d}t} \right]_{\text{aging}} = -\frac{1}{\tau_{\text{aging}}} N_{\text{fresh}}, \tag{1}$$

where N_{fresh} is the number concentration of fresh particles.

Before discussing the full set of sensitivity simulations in Sect. 3, we describe the particle-resolved simulation of aerosol dynamics in a baseline scenario and show how the aging timescale is used to quantify changes in per-particle CCN activity. The particle-resolved model is described in Sect. 2.1, and the κ-Köhler model (Petters and Kreidenweis, 2007) for computing CCN activity from the PartMC-MOSAIC data is discussed in Sect. 2.2. We discuss methods for computing aging timescales from the particle-resolved model output in Sect. 2.3.

2.1   Particle-resolved simulation of aerosol aging

The Particle Monte Carlo model (Riemer et al., 2009) coupled to the Model for Simulating Aerosol Interactions and Chemistry (Zaveri et al., 2008), PartMC-MOSAIC, is a Lagrangian box model that simulates gas and aerosol chemistry, gas-aerosol mass transfer, aerosol coagulation, gas and aerosol emissions, and dilution with background air. Coagulation events, particle emissions, and dilution with background air are simulated stochastically by PartMC, while gas- and aerosol-phase chemistry and gas-aerosol

mass transfer are simulated deterministically by MOSAIC. MOSAIC includes modules for gas-phase photochemistry (Zaveri and Peters, 1999), particle-phase thermodynamics (Zaveri et al., 2005a, b), and gas-particle mass transfer (Zaveri et al., 2008). The coupled model represents all atmospherically important aerosol species, including sulfate (SO_4), nitrate (NO_3), chloride (Cl), carbonate (CO_3), ammonium (NH_4), sodium (Na), calcium (Ca), methanesulfonic acid (MSA), black carbon (BC), primary organic aerosol (POA), and a number of secondary organic aerosol (SOA) species. A full description of the coupled model can be found in Riemer et al. (2009). PartMC-MOSAIC represents changes in particle composition by condensation and coagulation; we do not consider changes in particle shape or aging by photochemical oxidation. PartMC Version 2.1.4 was used to generate the results in this paper. Simulations were performed at a time step of 60 s, with approximately 10^5 computational particles.

We simulated 288 plume scenarios, varying meteorological conditions, emissions of gases and particles, and the background number concentration, with further description given in Sect. 3. The atmospheric composition and environmental conditions differed between the scenarios, but the general structure of all simulations was the same. In each case, we simulated a well-mixed air parcel that is advected over and away from large urban area. All scenarios started at 06:00 LST, at which time the parcel contained only background gas and aerosol without any freshly emitted particles. During transport over the urban area, the parcel received gas and aerosol emissions from 06:00 LST until 18:00 LST, after which all emissions ceased. In these scenarios, we simulate a well-mixed boundary layer during the day, and the parcel is assumed to be in the residual layer at night. The temperature, mixing height, and relative humidity were held constant. Before discussing the full set of scenarios in Sect. 3, we show changes in CCN activity and the diurnal evolution of aging timescales in a baseline scenario.

2.2 κ-Köhler model for computing CCN activity

We determined aging timescales from the particle-resolved results by tracking changes in CCN activity over two consecutive time steps. The equilibrium saturation ratio (S_i) over an aqueous droplet is computed through the κ-Köhler model (Köhler, 1936; Petters and Kreidenweis, 2007) as:

$$S_i(D_i) = \frac{D_i^3 - D_{\text{dry},i}^3}{D_i^3 - D_{\text{dry},i}^3 (1 - \kappa_i)} \exp\left(\frac{4\sigma_w M_w}{RT\rho_w D_i}\right), \tag{2}$$

where σ_w is the surface tension of water, M_w is the molecular weight of water, R is the universal gas constant, T is the ambient temperature, ρ_w is the density of water, D_i is the particle wet diameter, $D_{\text{dry},i}$ is the particle dry diameter, and κ_i is the hygroscopicity parameter introduced by Petters and Kreidenweis (2007). All other factors being equal, particles with a greater κ_i are more hygroscopic and more easily activated. The parameter κ has been determined empirically for a number of aerosol species (Table 1), and the effective hygroscopicity parameter κ_i for each particle is the volume-weighted average of κ for its constituent aerosol species. We denote the critical saturation ratio at which a particle activates and forms a cloud droplet with $S_{c,i}$ and the critical supersaturation as $s_{c,i} = (S(D_{c,i}) - 1) \times 100$.

Figure 1 shows the two-dimensional number density distribution as a function of the particle dry diameter ($D_{\text{dry},i}$) and the particle hygroscopicity parameter (κ_i). Choosing a certain environmental supersaturation threshold allows us to classify the particles as fresh or aged. For example, all particles to the left of the line for $s_{c,i} = 1\%$ are considered "fresh" for environmental supersaturations of 1 % or lower, and all particles to the right of the line for $s_{c,i} = 1\%$ are considered "aged" at supersaturations above 1 %. Only particles containing BC are shown in Fig. 1. In the scenarios presented in this study, all BC originated from diesel or gasoline exhaust.

The physical state of fresh emissions, prior to any aging, are shown in Fig. 1a, and changes in the distribution during two time periods are shown in Fig. 1b and c. Freshly

Explaining variance in BC aging timescales

L. Fierce et al.

Title Page

Abstract | Introduction

Conclusions | References

Tables | Figures

|◄ | ►|

◄ | ►

Back | Close

Full Screen / Esc

Printer-friendly Version

Interactive Discussion

emitted combustion particles are small and hydrophobic, with geometric mean diameter $D_{\text{dry,gm}} = 0.5\,\mu\text{m}$ and with a hygroscopicity parameter of $\kappa = 3 \times 10^{-4}$ or $\kappa = 8 \times 10^{-4}$ for particles from diesel or gasoline, respectively. Therefore, BC-containing particles are initially unable to activate at any $s < 1\%$ (lines in Fig. 1a). As $D_{\text{dry},i}$ and κ_i for individual particles increase by condensation and coagulation, their critical supersaturation $s_{\text{c},i}$ for CCN-active decreases, shown by particles crossing the lines of constant critical supersaturation in Fig. 1. Secondary aerosol forms through photochemical reactions during the day, causing rapid changes in particles' size and hygroscopicity. At night aging by condensation rates are slow, so coagulation is the dominant aging mechanism. This diurnal variation in aging rates is consistent with observations (Rose et al., 2011; Cheng et al., 2012). We define particles that "age" over a specific time period as those that transition from CCN-inactive to CCN-active, that is the particles that move from below a supersaturation line (CCN-inactive) at time t to above supersaturation line (CCN-active) at $t + \Delta t$.

2.3 CCN-based aging timescale

For the entire particle population, this change in the particle properties is quantified using the first-order aging timescale defined in Eq. (1). Because the time period Δt is short relative to the timescale τ_{aging}, Eq. (1) can be approximated as:

$$\left[\frac{dN_{\text{fresh}}}{dt}\right]_{\text{aging}} \approx -\frac{\Delta N_{\text{f}\to\text{a}}}{\Delta t}, \qquad (3)$$

where $\Delta N_{\text{f}\to\text{a}}$ is the number of discrete particles that transition from fresh at t to aged at $t + \Delta t$, calculated from changes in the number of fresh particles. Combining Eqs. (1) and (3), the aging timescale is computed as:

$$\tau_{\text{aging}}(t, s) \approx \Delta t \frac{N_{\text{fresh}}(t, s)}{\Delta N_{\text{f}\to\text{a}}(t, t + \Delta t, s)}. \qquad (4)$$

We refer to this aging timescale as the "bulk aging timescale" because it corresponds to the entire fresh particle population, and the term $\Delta N_{f \to a}$ includes all particles that transition from fresh to aged, regardless of their size. Later, we will introduce an analogous "size-resolved aging timescale". Further details on the derivation of the bulk aging timescale, including number balances for all processes affecting aging, are given in Riemer et al. (2010).

The temporal evolution of the timescale is shown for the baseline scenario in Fig. 2a at $s = 0.1\%$, $s = 0.3\%$, and $s = 1\%$. The gray shading corresponds to the time periods shown in Fig. 1. Particles must become highly hygroscopic to activate into cloud droplets at low s (e.g. $s = 0.1\%$) but require less processing to become CCN at higher values of s (e.g. $s = 1\%$), so the aging timescale tends to be shorter for higher values of s.

Any particle that transitions from fresh at t to aged at $t + \Delta t$ does so either by coagulation with a large, hygroscopic particle or by accumulating sufficient condensing material to become hygroscopic. The overall aging timescale τ_{aging} can be represented as the combination of separate timescales for aging by condensation τ_{cond} and by coagulation τ_{coag}:

$$\frac{1}{\tau_{\text{aging}}(t,s)} = \frac{1}{\tau_{\text{cond}}(t,s)} + \frac{1}{\tau_{\text{coag}}(t,s)}. \tag{5}$$

The contribution of condensation and coagulation to the overall aging timescale is shown by separate timescales for aging by condensation (τ_{cond}) and coagulation (τ_{coag}) at $s = 0.3\%$ in Fig. 2b. We computed the coagulation and condensation aging timescales by counting the number of particles that transition from fresh to aged after participating in a coagulation event, $\Delta N_{f \to a,\text{coag}}$, or that age only by condensation, $\Delta N_{f \to a,\text{cond}}$. Then, we applied Eq. (4) to find the corresponding condensation and coagulation aging timescales. Figure 2b shows that the overall aging timescale is shortest during the day (e.g. 1 h at $s = 0.3\%$) due to rapid condensation of semi-volatile sub-

Explaining variance in BC aging timescales

L. Fierce et al.

Title Page

Abstract	Introduction
Conclusions	References
Tables	Figures

|◄ | ►|

◄ | ►

Back | Close

Full Screen / Esc

Printer-friendly Version

Interactive Discussion

stances, and it is considerably longer at night (e.g. 24 h at $s = 0.3\%$), when coagulation is the dominant aging mechanism.

3   Sensitivity analysis

The results discussed in Sect. 2.3 are limited to only one scenario. We expect the aging timescale to vary depending on the local environmental conditions. For example, changes in the number and size distribution of background particles affects the rate at which they coagulate with BC-containing particles. In order to identify the set of independent variables that best explain variance in BC's aging timescale under a range of atmospheric conditions, we simulated aerosol dynamics in a series of plume scenarios and extracted aging timescales for each scenario. The environmental properties that affect aerosol dynamics varied diurnally and differed between scenarios (Table 2), causing the aging timescale to range from less than an hour (a large portion of particles age per time interval) to longer than a week (few particles age per time interval). The input parameters shown in Table 2 were selected to produce a comprehensive range of environmental conditions, consistent with observations described by Jimenez et al. (2009) and references therein. Simulations were performed using every combination of input parameters given in Table 2, leading to a total of 288 scenarios. Figure 3 shows the distribution of aerosol mass concentration for selected aerosol species for all scenarios simulated with PartMC-MOSAIC (black lines) and corresponding ambient observations compiled by Jimenez et al. (2009) (vertical colored lines), demonstrating that the range of conditions simulated in this set of scenarios is representative of the distribution in ambient concentrations.

Variance in the aging timescale is shown by the probability density distribution in Fig. 4. This figure was constructed from data at 10 min intervals in each of the 288 simulations. Distributions are shown for timescales computed at $s = 0.1\%$, $s = 0.3\%$, and $s = 1\%$. The supersaturation threshold s specifies the degree of change in particle properties required to classify a particle as aged, and timescales tend to decrease as s

Explaining variance in BC aging timescales

L. Fierce et al.

Title Page

Abstract	Introduction
Conclusions	References
Tables	Figures

◀   ▶

◀   ▶

Back   Close

Full Screen / Esc

Printer-friendly Version

Interactive Discussion

increases. In the following sections, we show that most of the variance in black carbon's aging timescale at a specific s is explained by only a few key variables.

3.1 Description of nonparametric regression

We identified the set of variables that best explain variance in the aging timescale through a nonparametric regression analysis, applying the kernel density regression introduced by Watson (1964) and Nadaraya (1964). A nonparametric regression was chosen, rather than a parametric regression, because we do not know a priori the shape of the predictor surface. The procedure in applying a nonparametric regression is as follows: (1) select a set of candidate independent variables to test; (2) use most of the data in the training set to find the expected value of the aging timescale as a function of the independent variables, as will be explained below; (3) evaluate this expected aging timescale using the rest of the data, called the testing set. The timescale from the regression is assessed by how well it predicts the values of the aging timescale in the testing set, represented by R^2. The purpose of this exploration is to find the independent variables that explain most of the variance in the aging timescale, indicated by the largest value of R^2. The advantage of this method is that it not only identifies the variables with the most influence, but also reveals the functional form.

To compute the expected value of the aging timescale we introduce the expected probability that a particle will age. In any simulation at any time t, a particle that is fresh at t may age between t and $t + \Delta t$ or it may remain fresh over that time period. Because these two events are mutually exclusive, this aging behavior may be represented by a binary variable $Y_{age,i}(t, t + \Delta t, s)$, where $Y_{age,i} = 1$ if the particle ages between t and $t + \Delta t$ and $Y_{age,i} = 0$ if it remains fresh.

The expected value of $Y_{age}(t, t + \Delta t, s)$ is computed as an average of $Y_{age,i}(t, t + \Delta t, s)$ for millions of individual particles in the training set, weighted according to the kernel function $K_h(x - x_i)$, where x is the independent variable of interest. The expected value

of $Y_{\text{age}}(t, t + \Delta t, s)$ is given by:

$$E[Y_{\text{age}}|x, s] = \frac{\sum\limits_{i=1}^{N_{\text{train}}} K_h(x - x_i(t)) Y_{\text{age},i}(t, t + \Delta t, s)}{\sum\limits_{j=1}^{N_{\text{train}}} K_h(x - x_i(t))}, \tag{6}$$

where x_i is the environmental variable at each time step in each simulation in the training set, evaluated for some target conditions x. The expected value of the aging timescale, $\hat{\tau}_{\text{aging}}(x)$, is then computed as a function of $E[Y_{\text{age}}|x, \Delta t, s]$:

$$\hat{\tau}_{\text{aging}}(x, s) = \frac{\Delta t}{E[Y_{\text{age}}|x, \Delta t, s]} \tag{7}$$

In this study we used a Gaussian kernel function with standard deviation h:

$$K_h\big(x - x_i(t)\big) = \frac{1}{\sqrt{2\pi}h} \exp\left(-\frac{(x - x_i(t))^2}{2h^2}\right). \tag{8}$$

The kernel function $K_h(x - x_i)$ defines the weight applied to each model timescale $\tau_{\text{age},i}$ to compute the expected timescale $\hat{\tau}_{\text{age}}$, such that timescales for conditions similar to the conditions of the target point are weighted most heavily in the regression. The regression function predicted by the kernel regression depends on the prescribed value for h, where larger h results in smoother regression functions. We applied Silverman's rule of thumb to select the value for h (Silverman, 1986), such that h depends on the number of independent variables, the standard deviation of each independent variable, and the total number of data points in the testing set.

Full Screen / Esc

Printer-friendly Version

Interactive Discussion

Explaining variance in BC aging timescales

L. Fierce et al.

Aging rates scale with the inverse of the aging timescale, so we quantified the portion of variance explained by the regression function, R^2, in terms of $1/\tau_{\text{aging}}$:

$$R^2(s) = 1 - \frac{\sum\limits_{j=1}^{N_{\text{test}}} N_{\text{fresh},j}(s)\left(\frac{1}{\hat{\tau}_{\text{aging},j}(s)} - \frac{1}{\tau_{\text{aging},j}(s)}\right)^2}{\sum\limits_{j=1}^{N_{\text{test}}} N_{\text{fresh},j}(s)\left(\frac{1}{\hat{\tau}_{\text{aging},j}(s)} - \frac{1}{\bar{\tau}_{\text{aging}}(s)}\right)^2}, \tag{9}$$

where N_{test} is the number of data points in the testing set, $\tau_{\text{aging},j}$ is the timescale from PartMC-MOSAIC, and $\hat{\tau}_{\text{aging},j}$ is the expected timescale from the regression for simulations in the testing set. The explained variance R^2 depends on the actual timescales $\tau_{\text{aging},j}$ from PartMC-MOSAIC, the expected aging timescales $\hat{\tau}_{\text{aging}}$ corresponding to the model conditions, and the mean across all timescales $\bar{\tau}_{\text{aging}}$ that are shown by vertical lines in Fig. 4.

We applied the kernel regression for different sets of independent variables and identified the minimal set of variables needed to explain most of the variance in BC's aging timescale. Condensation and coagulation are distinct aging processes that depend on different independent variables, so we perform the regression analysis for separate timescales τ_{cond} and τ_{coag}. For our application, we consider differences in the candidate environmental variables as well as differences in the characteristics of fresh (CCN-inactive) BC-containing particles. In the following section, we introduce a size-resolved aging timescale that captures differences in aging rates between particles of different sizes. Later, we show that the size distribution of fresh BC-containing particles strongly affects the condensation and coagulation aging timescales.

3.2 Size-resolved aging timescale

For a given set of environmental conditions, some fresh particles are more likely to age than others, and particles' tendency to age depends on their characteristics just prior

to the aging period. We evaluated how aging rates vary with a number of per-particle characteristics, such as particles' diameter at emission, their dry diameter just prior to aging, or their hygroscopicity parameter just prior to aging. We found that for given environmental conditions, per-particle aging rates were most correlated with the wet diameter of fresh (CCN-inactive) particles; that is, values of R^2 were greatest for regression functions that included the wet size distribution of fresh BC just prior to aging. Size-resolved aging timescales were computed at each time t and supersaturation s using the kernel regression described in the previous section. The expected value of Y_{age} for particles of wet diameter D was computed as the weighted average of $Y_{age,i}$ for all fresh particles $i = 1, \ldots, N_{p,fresh}$, computed at a specific t and s:

$$E\left[Y_{age}|D\right] = \frac{\sum\limits_{i=1}^{N_{p,fresh}} K_h(D - D_i(t))Y_{age,i}(t, t + \Delta t, s)}{\sum\limits_{i=1}^{N_{p,fresh}} K_h(D - D_i(t))}, \tag{10}$$

where the kernel weighting function $K_h(D - D_i)$ is a Gaussian (Eq. 8), such that fresh particles with D_i similar to the target diameter D are weighted most heavily in the regression. Similar to Eq. (7), the size-resolved aging timescale, $\tau_{aging}(D)$, is computed as a function of $E\left[Y_{age}|D\right]$ and the time step Δt:

$$\tau_{aging}(t, D, s) = \frac{\Delta t}{E\left[Y_{age}|t, \Delta t, D, s\right]}. \tag{11}$$

Weighting the size-resolved aging timescale by the size distribution of fresh BC-containing particles gives the bulk timescale that was defined in Eq. (4):

$$\tau_{aging}(t, s)^{-1} = \frac{\int_0^\infty \tau_{aging}(t, D, s)^{-1} n_{fresh}(t, D, s)\,\mathrm{d}D}{\int_0^\infty n_{fresh}(t, D, s)\,\mathrm{d}D}. \tag{12}$$

Full Screen / Esc

Printer-friendly Version

Interactive Discussion

By this relationship, the bulk aging timescale under a specific set of environmental conditions also varies with the size distribution of CCN-inactive (fresh) BC.

The temporal evolution of the size-resolved aging timescale is shown for the baseline scenario in the middle column of Fig. 5 for $s = 0.3\%$. The contributions of coagulation (Fig. 5b) and condensation (Fig. 5c) to the overall aging timescale (Fig. 5a) are shown by the separate size-resolved timescales for each process. The dominant mechanism driving the aging timescale depends on the time of day and the particle size.

A comparison between Fig. 5a and c shows that condensation was the dominant process driving diurnal variation in the size-resolved aging timescale. This diurnal pattern in condensation aging conditions is reflected in the bulk aging timescale shown in Fig. 2. The bulk condensation aging timescale was shorter than 4 h during the day for this scenario, and this was the dominant process affecting aging rates at this time. However, Fig. 5c shows that these rapid transitions from CCN-inactive to CCN-active occurred only for the largest ($D > 50$ nm) fresh particles, although condensation also caused an increase in D for smaller fresh particles. The coagulation aging timescale, on the other hand, was short for the smallest fresh particles and varied only slightly over the course of the simulation.

3.3 Independent variables that explain variance in BC's aging timescale

After exploring many combinations of independent variables in the regression analysis, we found that two variables, the size distribution of fresh BC ($n_{\text{fresh}}(D)$) and the number concentration of large, CCN-active particles ($N_{\text{CCN,large}}$), were needed to explain variance in the coagulation aging timescale (Fig. 6a). Three variables were needed to explain variance in the condensation aging timescale (Fig. 6b): the size distribution of fresh BC ($n_{\text{fresh}}(D)$); the flux of secondary aerosol ($\dot{f}_{\text{cond}}$), defined as the volume condensation rate of semi-volatile substances per particle surface area density; and the effective hygroscopicity parameter of secondary aerosol (κ_{cond}). The size distribution of fresh BC was included in each case by determining a regression for the size-resolved aging timescale before computing the bulk aging timescale according to Eq. (12).

Figure 6 shows the explained variance R^2 as a function of s for the independent variables that best explain variance in the condensation and coagulation aging timescales. Approximately 90 % of variance in the coagulation aging timescale was explained by regressions in terms of $n_{fresh}(D)$ and $N_{CCN,large}$ (black line of Fig. 6a). Brownian coagulation events are most likely to occur between large and small particles, so the coagulation aging timescale decreases when there are more particles that are CCN-active and are also large enough to be good coagulation partners. The smallest fresh particles are likely to coagulate with large background particles, where we found the threshold for "large" to be $D > 100$ nm by identifying the threshold that resulted in the highest R^2. A regression computed in terms of the number concentration of large particles (green line of Fig. 6a), rather than the number concentration of large and CCN-active particles, gave $R^2 \approx 85$ % at high supersaturation thresholds ($s > 0.8$ %) but $R^2 < 10$ % at low supersaturation thresholds ($s < 0.1$ %). This is because not all particles with $D > 100$ nm are CCN-active at $s = 0.1$ %, but nearly all particles that are CCN-active at this low s have $D > 100$ nm. On the other hand, if the independent variable was the number concentration of CCN-active particles (blue line of Fig. 6a), rather than the number concentration of large and CCN-active particles, $R^2 \approx 90$ % for timescales at low supersaturation thresholds ($s < 0.1$ %) and $R^2 \approx 70$ % at high supersaturation thresholds ($s > 0.8$ %). If the size distribution of fresh BC was neglected, R^2 ranged from 40 % to 60 %, depending on the supersaturation threshold (yellow line of Fig. 6a).

Whereas full regression in terms of $n_{fresh}(D)$, $\dot{f}_{cond}$, and κ_{cond} (black line of Fig. 6b) explained greater than 80 % of variances, R^2 was less than 60 % for regressions that did not include $n_{fresh}(D)$ (red line). Only 10–30 % of variance was explained if κ_{cond} was not included in the regression (grey line). If $\dot{f}_{cond}$ was not included, $R^2 \approx 0$ % for all s, regardless of the other variables included in the regression (not shown). This suggests, not surprisingly, that the condensation rate is the key variable driving aging by condensation, but the condensation aging timescale also depends strongly on the hygroscopicity of condensing aerosol κ_{cond} and on the size distribution of fresh particles $n_{fresh}(D)$.

The regression surfaces $\hat{\tau}_{coag}(N_{CCN,large}, D)$ and $\hat{\tau}_{cond}(\dot{f}_{cond}, \kappa_{cond}, D)$ are shown in Fig. 7a and b, respectively. Figure 7a shows that timescales for aging by coagulation range from hours to weeks. The coagulation aging timescale decreases with the number concentration of "large", CCN-active particles ($N_{CCN,large}$) and, for a given $N_{CCN,large}$, small BC-containing particles are more likely to age by coagulation than large BC-containing particles. On the other hand, condensation aging timescales are shortest for the largest fresh particles and, for these particles, the condensation aging timescale tends to decrease as $\dot{f}_{cond}$ or κ_{cond} increase. The two panels of Fig. 7b show $\hat{\tau}_{cond}$ as a function of $\dot{f}_{cond}$ and D for secondary aerosol with differing hygroscopicity, $\kappa_{cond} = 0.65$ on the left, representing secondary inorganic aerosol, and $\kappa_{cond} = 0.1$ on the right, representing secondary organic aerosol.

4 Discussion

Global models that employ first-order aging models assume a fixed timescale of 1–3 days, but observations show that aging timescales can be as short as a few hours in polluted areas (Zhang et al., 2008). Other modeling studies have suggested parameterizations that account for this variation in aging conditions. Riemer et al. (2004) evaluated aging timescales in a mesoscale model and parameterized timescales for aging by coagulation as a function of the overall number concentration. Pierce et al. (2009) developed an analytical expression that accounts for decreases in the number concentration of primary aerosol through coagulation events; for emitted particles of a specific size, the coagulation loss rate was computed by integrating the coagulation kernel over the entire background size distribution. However, the regression analysis applied in the current study reveals that 90 % of the variance in the coagulation aging timescale can be explained using a relatively simple representation of the background size distribution. We showed that the variation in the size-resolved aging timescales can be attributed to the number concentration of particles that are both large ($D > 100$ nm) and CCN-active. Other characteristics of the background size distributions are not needed.

Oshima and Koike (2013) developed a parameterization of the condensation aging timescale based on results from a box model, and, similar to the present study, computed aging timescales based on changes in CCN activity. However, unlike the present study, Oshima and Koike (2013) did not consider differences in the hygroscopic properties of the condensing material, and their aging timescale varied with the mass condensation rate per total BC mass concentration. In contrast, the regression analysis in the present study reveals that the volume condensation rate per overall aerosol surface area is the variable that best explains variance in BC's condensation aging timescale, which is consistent with laboratory studies (Zhang et al., 2008; Khalizov et al., 2009). The present work also differs from Oshima and Koike (2013) in the representation of the aerosol size distribution. Whereas Oshima and Koike (2013) parameterized bulk aging timescales for lognormal size distributions, we presented a size-resolved aging timescale that can be applied to any size distribution.

In order to compare the regression function of the size-resolved aging timescale that was presented in this work with the bulk aging timescales from other studies, we computed bulk aging timescales for two example BC populations under different combinations of aging conditions. Table 3 gives bulk aging timescales for four aging regimes, assuming freshly emitted BC has lognormal size distributions with a geometric mean diameter D_{gm} of 30 nm ("small" distribution cases) or 60 nm ("large" distribution cases). We found timescales on the order of a few hours under polluted conditions, consistent with observations, and the contribution of condensation or coagulation depended strongly on the size distribution of fresh BC. If the distribution contains a higher fraction of small particles ($D_{gm} = 30$ nm), the overall aging timescale at $s = 0.3\%$ is shorter than 3 h for particles evolving under high number concentrations ($N_{CCN,large} = 10\,000$ cm^{-3}) and, under these conditions, the value of the aging timescale is relatively insensitive to $\dot{f}_{cond}$. On the other hand, the overall aging timescale at $s = 0.3\%$ is shorter than 3 h for large fresh particles ($D_{gm} = 60$ nm) only if particles age under conditions of rapid secondary aerosol condensation ($\dot{f}_{cond} = 1$ nm h^{-1}) and, for these high values of $\dot{f}_{cond}$, the aging timescale is insensitive to $N_{CCN,large}$.

As in all relationships for BC's aging timescale, the value of the aging timescale depends strongly on the criterion used to distinguish fresh and aged particles. Particle activation at a specific environmental supersaturation is the aging criterion applied in this study, representing changes in particle characteristics that most affect their susceptibility to wet deposition. Table 3 shows that the value of the aging timescale depends strongly on the criterion supersaturation at which CCN activation was evaluated, consistent with Riemer et al. (2010) and Oshima and Koike (2013). Further, the relative importance of condensation versus coagulation as aging processes also depends on the supersaturation threshold.

5   Conclusions

This study identifies the minimal set of independent variables needed to explain variance in black carbon's aging timescale. We simulated the evolution of gases and aerosols in a series of urban scenarios with the particle-resolved model PartMC-MOSAIC and extracted time-dependent aging timescales based on the rate at which individual particles transition from CCN-inactive to CCN-active at a specified environmental supersaturation. The value of the aging timescale spanned orders of magnitude, depending on local environmental conditions and the supersaturation threshold at which CCN activity was evaluated. Aging timescales were shorter than an hour under conditions of rapid secondary aerosol formation, but on the order of days in the absence of secondary aerosol precursors. Condensation aging timescales exhibited more variation than coagulation aging timescales, and the relative importance of each aging mechanism depended on the size range of particles to be aged. We performed a non-parametric regression analysis on model data from 288 scenarios in order to identify the independent variables with which aging timescales are best correlated and quantified the portion of variance explained by regressions in terms of these variables.

To our knowledge, this is the first study to apply a regression analysis to identify the minimal set of parameters needed to explain variance in black carbon aging rates.

Full Screen / Esc

Printer-friendly Version

Interactive Discussion

After evaluating a number of independent variables, we found that the flux of secondary aerosol, the hygroscopicity of secondary aerosol, and the size distribution of CCN-inactive (fresh) BC-containing particles were the minimal set of parameters needed to explain 80 % of variance in the condensation aging timescale. On the other hand, 90 % of variance in the coagulation aging timescale was explained by only two variables: the size distribution of fresh BC-containing particles and the number concentration of particles that are both large ($D > 100$ nm) and CCN-active. This work distills the complex interactions captured by the particle-resolved model to a few input variables, all of which are tracked by existing global climate models, and is a first step toward developing physically-based parameterizations of aerosol aging.

References

Ackerman, A., Toon, O., Stevens, D., Heymsfield, A., Ramanathan, V., and Welton, E.: Reduction of tropical cloudiness by soot, Science, 288, 1042–1047, 2000. 18704

Albrecht, B.: Aerosols, cloud microphysics, and fractional cloudiness, Science, 245, 1227–1230, 1989. 18704

Bauer, S. E., Wright, D. L., Koch, D., Lewis, E. R., McGraw, R., Chang, L.-S., Schwartz, S. E., and Ruedy, R.: MATRIX (Multiconfiguration Aerosol TRacker of mIXing state): an aerosol microphysical module for global atmospheric models, Atmos. Chem. Phys., 8, 6003–6035, doi:10.5194/acp-8-6003-2008, 2008. 18705

Binkowski, F. and Roselle, S.: Models-3 community multiscale air quality (CMAQ) model aerosol component: 1. Model description, J. Geophys. Res., 108, 4183, doi:10.1029/2001JD001409, 2003. 18705

Cantrell, W., Shaw, G., Cass, G., Chowdhury, Z., Hughes, L., Prather, K., Guazzotti, S., and Coffee, K.: Closure between aerosol particles and cloud condensation nuclei at Kaashidhoo Cli-

Explaining variance in BC aging timescales

L. Fierce et al.

Title Page

Abstract | Introduction

Conclusions | References

Tables | Figures

◀ | ▶

◀ | ▶

Back | Close

Full Screen / Esc

Printer-friendly Version

Interactive Discussion

mate Observatory, J. Geophys. Res., 106, 28711–28718, doi:10.1029/2000JD900781, 2001. 18705

Cheng, Y. F., Su, H., Rose, D., Gunthe, S. S., Berghof, M., Wehner, B., Achtert, P., Nowak, A., Takegawa, N., Kondo, Y., Shiraiwa, M., Gong, Y. G., Shao, M., Hu, M., Zhu, T., Zhang, Y. H., Carmichael, G. R., Wiedensohler, A., Andreae, M. O., and Pöschl, U.: Size-resolved measurement of the mixing state of soot in the megacity Beijing, China: diurnal cycle, aging and parameterization, Atmos. Chem. Phys., 12, 4477–4491, doi:10.5194/acp-12-4477-2012, 2012. 18710

Chin, M., Diehl, T., Tan, Q., Prospero, J. M., Kahn, R. A., Remer, L. A., Yu, H., Sayer, A. M., Bian, H., Geogdzhayev, I. V., Holben, B. N., Howell, S. G., Huebert, B. J., Hsu, N. C., Kim, D., Kucsera, T. L., Levy, R. C., Mishchenko, M. I., Pan, X., Quinn, P. K., Schuster, G. L., Streets, D. G., Strode, S. A., Torres, O., and Zhao, X.-P.: Multi-decadal aerosol variations from 1980 to 2009: a perspective from observations and a global model, Atmos. Chem. Phys., 14, 3657–3690, doi:10.5194/acp-14-3657-2014, 2014. 18706

Clegg, S., Brimblecombe, P., and Wexler, A.: Thermodynamic model of the system H^+-NH_4^+-SO_4^{2-}-NO_3^--H_2O at tropospheric temperatures, J. Phys. Chem. A, 102, 2137–2154, 1998. 18728

Cooke, W. and Wilson, J.: A global black carbon aerosol model, J. Geophys. Res., 101, 19395–19409, doi:10.1029/96JD00671, 1996. 18705

Cozic, J., Verheggen, B., Mertes, S., Connolly, P., Bower, K., Petzold, A., Baltensperger, U., and Weingartner, E.: Scavenging of black carbon in mixed phase clouds at the high alpine site Jungfraujoch, Atmos. Chem. Phys., 7, 1797–1807, doi:10.5194/acp-7-1797-2007, 2007. 18705

Croft, B., Lohmann, U., and von Salzen, K.: Black carbon ageing in the Canadian Centre for Climate modelling and analysis atmospheric general circulation model, Atmos. Chem. Phys., 5, 1931–1949, doi:10.5194/acp-5-1931-2005, 2005. 18705, 18706

Furutani, H., Dallsto, M., Roberts, G., and Prather, K.: Assessment of the relative importance of atmospheric aging on CCN activity derived from field observations, Atmos. Environ., 42, 3130–3142, 2008. 18705

Hansen, J. and Nazarenko, L.: Soot climate forcing via snow and ice albedos, P. Natl. Acad. Sci. USA, 101, 423–428, doi:10.1073/pnas.2237157100, 2004. 18704

Jacobson, M.: Development and application of a new air pollution modeling system – II. Aerosol module structure and design, Atmos. Environ., 31, 131–144, 1997. 18705

Title Page

Abstract | Introduction

Conclusions | References

Tables | Figures

|◄ | ►|

◄ | ►

Back | Close

Full Screen / Esc

Printer-friendly Version

Interactive Discussion

Jacobson, M. Z.: Climate response of fossil fuel and biofuel soot, accounting for soot's feed-back to snow and sea ice albedo and emissivity, J. Geophys. Res.-Atmos., 109, D21201, doi:10.1029/2004JD004945, 2004. 18704

Jimenez, J. L., Canagaratna, M. R., Donahue, N. M., Prevot, A. S. H., Zhang, Q., Kroll, J. H., DeCarlo, P. F., Allan, J. D., Coe, H., Ng, N. L., Aiken, A. C., Docherty K. S., Ulbrich, I. M., Grieshop, A. P., Robinson, A. L., Duplissy, J., Smith, J. D., Wilson, K. R., Lanz, V. A., Hueglin, C., Sun, Y. L., Tian, J., Laaksonen, A. Raatikainen, T., Rautiainen, J., Vaatto-vaara, P., Ehn, M., Kulmala, M., Tomlinson, J. M., Collins, D. R., Cubison, M. J., Dun-lea, E. J., Huffman, J. A., Onasch, T. B., Alfarra, M. R., Williams, P. I., Bower, K., Kondo, Y., Schneider, J., Drewnick, F., Borrmann, S., Weimer, S., Demerjian, K., Salcedo, D., Cot-trell, L., Griffin, R., Takami, A., Miyoshi, T., Hatakeyama, S., Shimono, A., Sun, J. Y., Zhang, Y. M., Dzepina, K,Kimmel, J. R., Sueper D., Jayne, J. T., Herndon, S. C., Trim-born, A. M., Williams, L. R., Wood, E. C., Middlebrook, A. M. Kolb, C. E., Baltensperger, U., and Worsnop, D. R.: Evolution of organic aerosols in the atmosphere, Science, 326, 1525–1529, 2009. 18712

Jo, D., Park, R., Kim, M., and Spracklen, D.: Effects of chemical aging on global secondary organic aerosol using the volatility basis set approach, Atmos. Environ., 81, 230–244, 2013. 18706

Johnson, K., Zuberi, B., Molina, L., Molina, M., Iedema, M., Cowin, J., Gaspar, D., Wang, C., and Laskin, A.: Processing of soot in an urban environment: case study from the Mexico City Metropolitan Area, Atmos. Chem. Phys., 5, 3033–3043, 2005, http://www.atmos-chem-phys.net/5/3033/2005/. 18705

Khalizov, A. F., Zhang, R., Zhang, D., Xue, H., Pagels, J., and McMurry, P. H.: Formation of highly hygroscopic soot aerosols upon internal mixing with sulfuric acid vapor, J. Geophys. Res.-Atmos., 114, D05208, doi:10.1029/2008JD010595, 2009. 18720

Koch, D.: Transport and direct radiative forcing of carbonaceous and sulfate aerosols in the giss gcm, J. Geophys. Res.-Atmos., 106, 20311–20332, 2001. 18705

Koch, D., Schulz, M., Kinne, S., McNaughton, C., Spackman, J. R., Balkanski, Y., Bauer, S., Berntsen, T., Bond, T. C., Boucher, O., Chin, M., Clarke, A., De Luca, N., Dentener, F., Diehl, T., Dubovik, O., Easter, R., Fahey, D. W., Feichter, J., Fillmore, D., Freitag, S., Ghan, S., Ginoux, P., Gong, S., Horowitz, L., Iversen, T., Kirkevåg, A., Klimont, Z., Kondo, Y., Krol, M., Liu, X., Miller, R., Montanaro, V., Moteki, N., Myhre, G., Penner, J. E., Perlwitz, J., Pitari, G., Reddy, S., Sahu, L., Sakamoto, H., Schuster, G., Schwarz, J. P., Seland, Ø., Stier, P.,

Title Page

Abstract · Introduction

Conclusions · References

Tables · Figures

|◄ · ►|

◄ · ►

Back · Close

Full Screen / Esc

Printer-friendly Version

Interactive Discussion

Takegawa, N., Takemura, T., Textor, C., van Aardenne, J. A., and Zhao, Y.: Evaluation of black carbon estimations in global aerosol models, Atmos. Chem. Phys., 9, 9001–9026, doi:10.5194/acp-9-9001-2009, 2009. 18705

Köhler, H.: The nucleus in and the growth of hygroscopic droplets, T. Faraday Soc., 32, 1152–1161, 1936. 18709

Liu, J., Fan, S., Horowitz, L. W., and Levy, H.: Evaluation of factors controlling long-range transport of black carbon to the arctic, J. Geophys. Res.-Atmos., 116, D04307, doi:10.1029/2010JD015145, 2011. 18705

Lohmann, U. and Feichter, J.: Global indirect aerosol effects: a review, Atmos. Chem. Phys., 5, 715–737, doi:10.5194/acp-5-715-2005, 2005. 18704

Maricq, M. M.: Chemical characterization of particulate emissions from diesel engines: a review, J. Aerosol Sci., 38, 1079–1118, 2007. 18705

McCormick, R. A. and Ludwig, J. H.: Climate modification by atmospheric aerosols, Science, 156, 1358–1359, 1967. 18704

McGraw, R.: Description of aerosol dynamics by the quadrature method of moments, Aerosol Sci. Tech., 27, 255–265, 1997. 18705

Nadaraya, E. A.: On estimating regression, Theor. Probab. Appl., 9, 141–142, 1964. 18713

Oshima, N. and Koike, M.: Development of a parameterization of black carbon aging for use in general circulation models, Geosci. Model Dev., 6, 263–282, doi:10.5194/gmd-6-263-2013, 2013. 18705, 18720, 18721

Petters, M., Prenni, A., Kreidenweis, S., DeMott, P., Matsunaga, A., Lim, Y., and Ziemann, P.: Chemical aging and the hydrophobic-to-hydrophilic conversion of carbonaceous aerosol, Geophys. Res. Lett., 33, L24806, doi:10.1029/2006GL027249, 2006. 18728

Petters, M. D. and Kreidenweis, S. M.: A single parameter representation of hygroscopic growth and cloud condensation nucleus activity, Atmos. Chem. Phys., 7, 1961–1971, doi:10.5194/acp-7-1961-2007, 2007. 18707, 18709, 18728

Pierce, J., Theodoritsi, G., Adams, P., and Pandis, S.: Parameterization of the effect of sub-grid scale aerosol dynamics on aerosol number emission rates, J. Aerosol Sci., 40, 385–393, 2009. 18706, 18719

Prenni, A., Petters, M., Kreidenweis, S., DeMott, P., and Ziemann, P.: Cloud droplet activation of secondary organic aerosol, J. Geophys. Res., 112, 10223, doi:10.1029/2006JD007963, 2007. 18728

Title Page

Abstract | Introduction

Conclusions | References

Tables | Figures

|◄ | ►|

◄ | ►

Back | Close

Full Screen / Esc

Printer-friendly Version

Interactive Discussion

Riemer, N., Vogel, H., and Vogel, B.: Soot aging time scales in polluted regions during day and night, Atmos. Chem. Phys., 4, 1885–1893, doi:10.5194/acp-4-1885-2004, 2004. 18706, 18719

Riemer, N., West, M., Zaveri, R., and Easter, R.: Simulating the evolution of soot mixing state with a particle-resolved aerosol model, J. Geophys. Res., 114, D09202, doi:10.1029/2008JD011073, 2009. 18707, 18708

Riemer, N., West, M., Zaveri, R., and Easter, R.: Estimating black carbon aging time-scales with a particle-resolved aerosol model, J. Aerosol Sci., 41, 143–158, 2010. 18706, 18711, 18721

Rose, D., Gunthe, S. S., Su, H., Garland, R. M., Yang, H., Berghof, M., Cheng, Y. F., Wehner, B., Achtert, P., Nowak, A., Wiedensohler, A., Takegawa, N., Kondo, Y., Hu, M., Zhang, Y., Andreae, M. O., and Pöschl, U.: Cloud condensation nuclei in polluted air and biomass burning smoke near the mega-city Guangzhou, China – Part 2: Size-resolved aerosol chemical composition, diurnal cycles, and externally mixed weakly CCN-active soot particles, Atmos. Chem. Phys., 11, 2817–2836, doi:10.5194/acp-11-2817-2011, 2011. 18710

Rosen, H., Hansen, A., Gundel, L., and Novakov, T.: Identification of the optically absorbing component in urban aerosols, Appl. Optics, 17, 3859–3861, 1978. 18704

Schmidt, G. A., Kelley, M., Nazarenko, L., Ruedy, R., Russell, G. L., Aleinov, I., Bauer, M. Bauer, S. E., Bhat, M. K., Bleck, R., Canuto, V., Chen, Y. H., Cheng, Y., Clune, T. L., Del Genio, A., de Fainchtein, R., Faluvegi, G., Hansen, J. E., Healy, R. J., Kiang, N. Y., Koch, D. Lacis, A. A., LeGrande, A. N., Lerner, J., Lo, K. K. Matthews, E. E., Menon, S., Miller, R. L., Oinas, V., Oloso, A. O., Perlwitz, J. P., Puma, M. J., Putman, W. M., Rind, D., Romanou, A., Sato, M., Shindell, D. T., Sun, S., Syed, R. A., Tausnev, N., Tsigaridis, K., Unger, N., Voulgarakis, A., Yao, M.-S., and Zhang, J.: Configuration and assessment of the GISS ModelE2 contributions to the CMIP5 archive, J. Adv. Model. Earth Syst., 6, 141–184, doi:10.1002/2013MS000265, 2014. 18706

Schulz, M., Textor, C., Kinne, S., Balkanski, Y., Bauer, S., Berntsen, T., Berglen, T., Boucher, O., Dentener, F., Guibert, S., Isaksen, I. S. A., Iversen, T., Koch, D., Kirkevåg, A., Liu, X., Montanaro, V., Myhre, G., Penner, J. E., Pitari, G., Reddy, S., Seland, Ø., Stier, P., and Takemura, T.: Radiative forcing by aerosols as derived from the AeroCom present-day and pre-industrial simulations, Atmos. Chem. Phys., 6, 5225–5246, doi:10.5194/acp-6-5225-2006, 2006. 18704

Explaining variance in BC aging timescales

L. Fierce et al.

Title Page

Abstract | Introduction

Conclusions | References

Tables | Figures

|◄ | ►|

◄ | ►

Back | Close

Full Screen / Esc

Printer-friendly Version

Interactive Discussion

Silverman, B.: Density Estimation for Statistics and Data Analysis, vol. 26, Chapman & Hall/CRC, New York, 1986. 18714

Svenningsson, B., Rissler, J., Swietlicki, E., Mircea, M., Bilde, M., Facchini, M. C., Decesari, S., Fuzzi, S., Zhou, J., Mønster, J., and Rosenørn, T.: Hygroscopic growth and critical super-saturations for mixed aerosol particles of inorganic and organic compounds of atmospheric relevance, Atmos. Chem. Phys., 6, 1937–1952, doi:10.5194/acp-6-1937-2006, 2006. 18728

Twomey, S.: The influence of pollution on the shortwave albedo of clouds, J. Atmos. Sci., 34, 1149–1152, 1977. 18704

Twomey, S., Piepgrass, M., and Wolfe, T.: An assessment of the impact of pollution on global cloud albedo, Tellus B, 36, 356–366, 1984. 18704

Watson, G. S.: Smooth regression analysis, Sankhya Ser. A, 26, 359–372, 1964. 18713

Weingartner, E., Burtscher, H., and Baltensperger, U.: Hygroscopic properties of carbon and diesel soot particles, Atmos. Environ., 31, 2311–2327, 1997. 18705

Wexler, A., Lurmann, F., and Seinfeld, J.: Modelling urban and regional aerosols–i. model development, Atmos. Environ., 28, 531–546, 1994. 18705

Zaveri, R. and Peters, L.: A new lumped structure photochemical mechanism for large-scale applications, J. Geophys. Res., 104, 30387–30415, doi:10.1029/1999JD900876, 1999. 18708

Zaveri, R., Easter, R., and Peters, L.: A computationally efficient multicomponent equilibrium solver for aerosols (MESA), J. Geophys. Res., 110, D24203, doi:10.1029/2004JD005618, 2005a. 18708

Zaveri, R., Easter, R., and Wexler, A.: A new method for multicomponent activity coefficients of electrolytes in aqueous atmospheric aerosols, J. Geophys. Res., 110, D02201, doi:10.1029/2004JD005618, 2005b. 18708

Zaveri, R., Easter, R., Fast, J., and Peters, L.: Model for simulating aerosol interactions and chemistry (MOSAIC), J. Geophys. Res., 113, D13204, doi:10.1029/2007JD008782, 2008. 18707, 18708

Zhang, R., Khalizov, A. F., Pagels, J., Zhang, D., Xue, H., and McMurry, P. H.: Variability in morphology, hygroscopicity, and optical properties of soot aerosols during atmospheric processing, P. Natl. Acad. Sci. USA, 105, 10291–10296, 2008. 18719, 18720

Zuberi, B., Johnson, K., Aleks, G., Molina, L., Molina, M., and Laskin, A.: Hydrophilic properties of aged soot, Geophys. Res. Lett., 32, L01807, doi:10.1029/2004GL021496, 2005. 18705

Explaining variance in BC aging timescales

L. Fierce et al.

Title Page

Abstract	Introduction
Conclusions	References
Tables	Figures

|◄ | ►|

◄ | ►

Back | Close

Full Screen / Esc

Printer-friendly Version

Interactive Discussion

Table 1. Hygroscopicity parameter assigned to aerosol species

aerosol species	κ_i	citation
NO_3	0.65	Clegg et al. (1998); Svenningsson et al. (2006); Petters and Kreidenweis (2007)
SO_4	0.65	Clegg et al. (1998); Svenningsson et al. (2006); Petters and Kreidenweis (2007)
NH_4	0.65	Clegg et al. (1998); Svenningsson et al. (2006); Petters and Kreidenweis (2007)
SOA	0.1	Prenni et al. (2007)
BC	0	Petters et al. (2006)
OC	0.001	Petters et al. (2006)

Table 2. Input parameters varied in series of plume scenarios

input parameter	values assigned
gas-phase emissions	varied precursors for NH_4NO_3, $(NH_4)_2SO_4$, both NH_4NO_3 and $(NH_4)_2SO_4$, SOA
latitude	5° N, 40° N, 60° N
season	summer, winter
BC emission rate ($m^{-2}\,s^{-1}$)	3.2×10^7, 1.6×10^8, 3.2×10^8
background num. conc. (m^{-3})	1.65×10^9, 3.3×10^9
relative humidity	40 %, 95 %

Table 3. Bulk aging timescale for two fresh particle size distributions under different aging regimes. Condensation, coagulation, and overall aging timescales are given for $s = 0.3\%$, and overall aging timescales are given for $s = 0.1\%$ and $s = 1\%$. We assumed lognormal size distributions of fresh BC with a geometric standard deviation of 1.7.
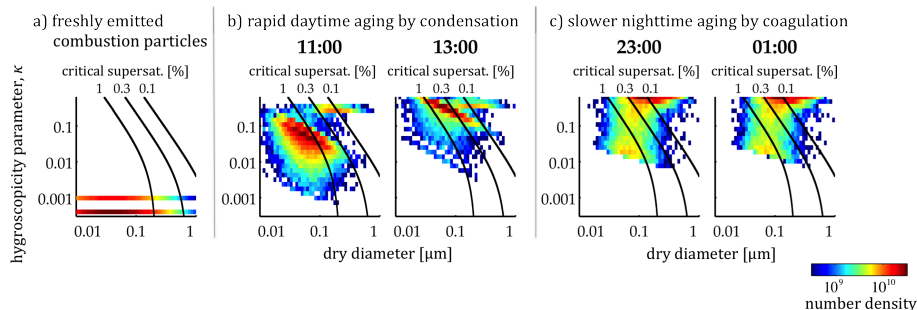
| D_{gm} [nm]	$\dot{f}_{cond}$ [nm h^{-1}]	$N_{CCN,large}$ [cm^{-3}]	$s = 0.3\%$ $\hat{\tau}_{cond}$ [h]	$\hat{\tau}_{coag}$ [h]	$\hat{\tau}_{age}$ [h]	$s = 0.1\%$ $\hat{\tau}_{age}$ [h]	$s = 1\%$ $\hat{\tau}_{age}$ [h]
30	0.01	500	460	17	16	63	21
60	0.01	500	44	40	20	154	9
30	1	500	18	17	9	2.5	0.2
60	1	500	2.8	40	2.6	5	0.5
30	0.01	10 000	460	5	5	7	4
60	0.01	10 000	44	6	5.4	21	5
30	1	10 000	18	2.6	2.2	5	0.4
60	1	10 000	2.8	6	2	4.5	0.3

Figure 1. Two-dimensional probability density distribution shows changes in particle properties. As particles increase in size (horizontal axis) and hygroscopicity (vertical axis), they are able to activate at lower critical supersaturation thresholds (superimposed lines). **(a)** Freshly emitted particles are hydrophobic, with $\kappa = 3 \times 10^{-4}$ and $\kappa = 8 \times 10^{-4}$ for diesel and gasoline, respectively. **(b)** During the daytime, particles age rapidly by condensation of semi-volatile substances that are produced through photochemical reactions. **(c)** At night, condensation aging is slow, and particles age only by coagulation.
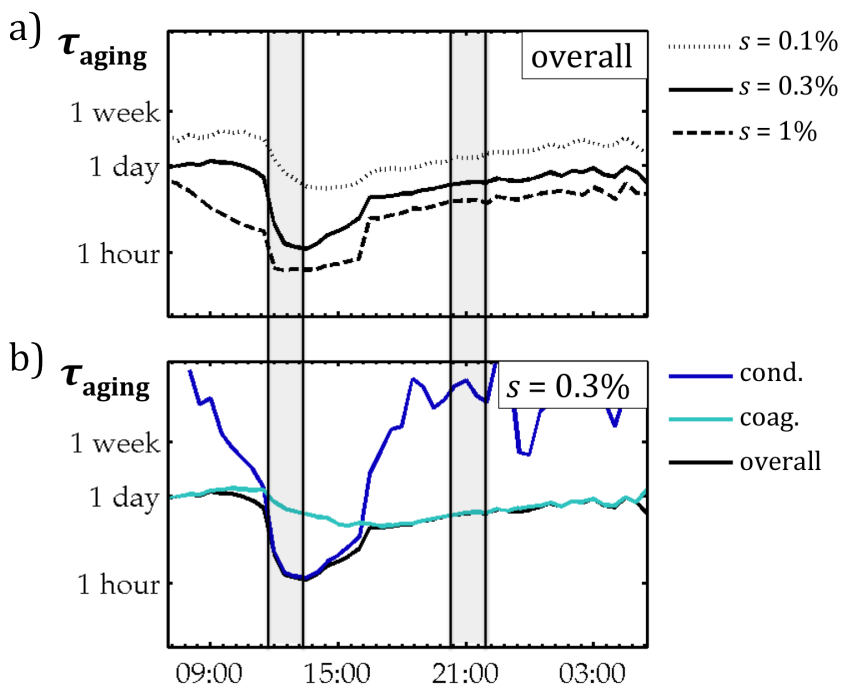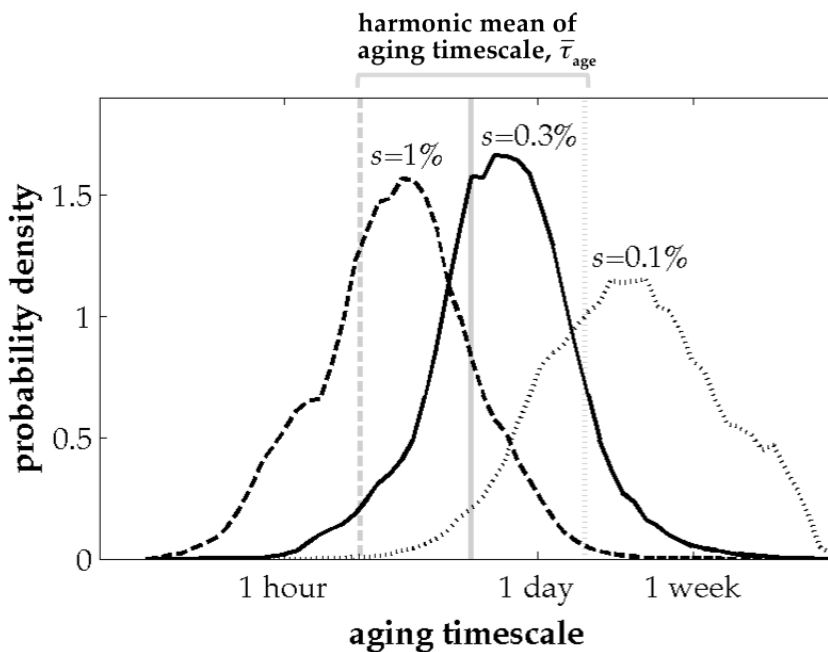
Figure 2. For a single scenario, temporal evolution of **(a)** overall aging timescale at $s = 0.1\%$, $s = 0.3\%$, and $s = 1\%$ and **(b)** overall, condensation, and coagulation aging timescales at $s = 0.3\%$. The shaded regions show how the value of the aging timescale reflects changes in per-particle characteristics, which correspond to Fig. 1. Short aging timescales correspond to rapid increases in particle size and hygroscopicity (Fig. 1b), and long aging timescales correspond to slow changes in particle properties (Fig. 1c).

Figure 3. Probability density function of aerosol mass species in simulations (black line in each graph) show that model cases represent variation in atmospheric conditions from ambient observations (vertical colored lines). Probability density functions include all output time steps in the full ensemble of sensitivity simulations.

Full Screen / Esc

Printer-friendly Version

Interactive Discussion

Figure 4. Probability density function of aging timescales for the full ensemble of sensitivity simulations, computed at three environmental supersaturation levels: $s = 0.1\%$, $s = 0.3\%$, and $s = 1\%$.
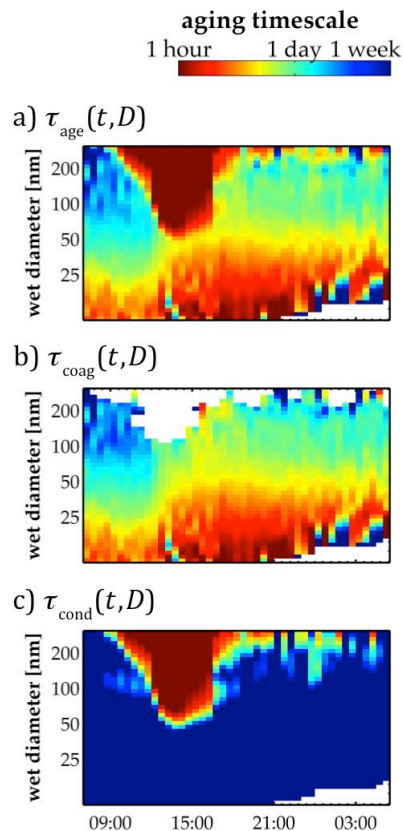
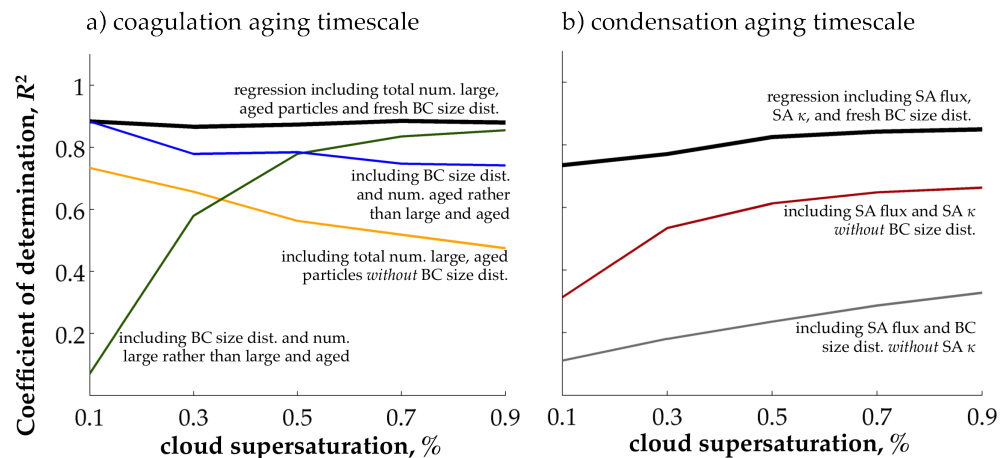**Explaining variance in BC aging timescales**

L. Fierce et al.

Figure 5. For baseline scenario, **(a)** overall size-dependent aging timescale, **(b)** condensation aging timescale, and **(c)** coagulation aging timescale. Values are shown for $s = 0.3\%$.

Figure 6. Coefficient of determination for **(a)** condensation and **(b)** coagulation timescales as a function of supersaturation for selected combinations of independent variables. For all s, approximately 90 % of variance in coagulation aging timescale is explained by two independent variables **(a)**, and 80 % of variance in condensation aging timescale is explained by three independent **(b)**.

Figure 7. Coagulation aging timescale as a function of wet diameter and number of large, CCN-active particles **(a)** and condensation aging timescale as a function of wet diameter, secondary aerosol flux, and hygroscopicity of secondary aerosol **(b)**. Results are shown for a threshold supersaturation s of 0.3 %.